Ceramics International 44 (2018) 2959–2967

Contents lists available at ScienceDirect

Ceramics International

journal homepage: www.elsevier.com/locate/ceramint

Effects of Y-TZP blank manufacturing control and addition of TiO_2 nanotubes on structural reliability of dental materials

Ana Paula Rodrigues Magalhães[a], Carlos Alberto Fortulan[b], Paulo Noronha Lisboa-Filho[c], Carla Müller Ramos-Tonello[a], Orisson Ponce Gomes[c], Paulo Francisco Cesar[d], Karen Akemi Fukushima[d], Rafael Francisco Lia Mondelli[a], Ana Flávia Sanches Borges[a,*]

[a] Department of Operative Dentistry, Endodontics and Dental Materials, Bauru School of Dentistry, University of São Paulo (USP), Al. Octávio Pinheiro Brisola, 9-75, Vila Universitária, 17012-901 Bauru, SP, Brazil
[b] Department of Mechanical Engineering, University of São Paulo (USP), Avenida dos Trabalhadores São-carlense, 400, Parque Arnold Schimidt, 13566-590 São Carlos, SP, Brazil
[c] Physics Department, Faculty of Sciences, State University of São Paulo (UNESP), Av. Eng. Luís Edmundo Carrijo Coube, 14, Nucleo Res. Pres. Geisel, 17033-360 Bauru, SP, Brazil
[d] Department of Biomaterials and Oral Biology, University of São Paulo (USP), Av. Prof. Lineu Prestes, 2227, Vila Universitaria, 05508-000 São Paulo, SP, Brazil

ARTICLE INFO

Keywords:
Nanocomposites (B)
TiO_2 (D)
ZrO_2 (D)
Biomedical applications (E)

ABSTRACT

Titanium dioxide (TiO_2) nanotubes have been applied to enhance the mechanical and biological properties of dental materials. Yttria-stabilized tetragonal zirconia polycrystals (Y-TZP) have been increasingly used in dentistry as a substructure for crowns and fixed partial prostheses. Aside from its optimal clinical results, Y-TZP is prone to failures due to microstructure-related defects introduced in the manufacturing process that may lower its structural and clinical reliability. The purpose of this study was to evaluate the role of the manufacturing process of blanks as well as their original composition modification by addition of TiO_2 nanotubes (0%, 1%, 2% and 5% in volume) while controlling all manufacturing steps. Materials were subjected to a biaxial flexural strength test, a fractographic qualitative analysis by scanning electron microscopy (SEM), a microstructure evaluation in field emission-SEM and X-ray diffraction. Values of flexural strength were subjected to ANOVA, Tukey ($\alpha = 0.05$) and Weibull statistics. Grain size values were subjected to Kruskal-Wallis and Dunn tests ($\alpha = 0.05$). Highlights of the results include that for experimental Y-TZP added 2% vol TiO_2 nanotube ceramics presented flexural strength values at 577 MPa and Weibull modulus (m) at 8.1. The addition of TiO_2 nanotubes in different blends influenced experimental Y-TZP properties, leading to lower flexural strength, although they presented higher m than the commercial Y-TZP. Nanotubes also led to bigger grain sizes, more pores and a slight increase in the monoclinic phase, influencing the microstructure of Y-TZP. Y-TZP blank manufacturing control as well as addition of TiO_2 nanotubes led to higher m values and, hence, greater structural reliability.

1. Introduction

Ceramics have been used in dentistry more in recent years, and their types and applications are constantly expanding. Ceramics generally are inorganic, nonmetallic solids synthesized by heat treatment and subsequent cooling [1,2]. Currently, the word “ceramic” refers to materials such as glass, advanced ceramics and cement systems [2], leading to a much broader meaning. High-strength oxide ceramic materials, such as zirconium dioxide (ZrO_2), have many different applications such as extrusion dyes, valves and port liners for combustion engines and low corrosion and thermal shock resistant refractory liners [3].

Zirconia stabilized with the addition of yttrium oxide, the so-called yttria-stabilized tetragonal zirconia polycrystal (Y-TZP), becomes a high-strength ceramic with enhanced mechanical properties and higher biological stability [2,4]. Y-TZP has been increasingly used in dentistry as a core material for dental crowns and fixed dental prostheses. Compared to other dental ceramics, zirconia-based ones generally present enhanced mechanical properties, such as a higher Young's modulus, flexural strength, fracture toughness and hardness [3,5],

Abbreviations: ANOVA, analysis of variance; cc, compression curls; EDX, Energy Dispersive X-Ray Spectroscopy; FE-SEM, Field Emission Scanning Electron Microscopy; hl, hackle lines; ISO, International Organization for Standardization; m, mirror region; m, Weibull modulus; p, pores; PMMA, Polymethyl methacrylate; SD, standard deviation; SEM, Scanning Electron Microscope; TEM, Transmission Electron Microscopy; wh, wake hackle lines; XRD, X-ray diffraction; Y-TZP, Yttria-stabilized tetragonal zirconia polycrystal; σ_0, characteristic strength

* Correspondence to: Bauru School of Dentistry, University of São Paulo, Al. Octávio Pinheiro Brisola, 9–75, Vila Universitária, 17012-901 Bauru, SP, Brazil.
E-mail address: afborges@fob.usp.br (A.F.S. Borges).

https://doi.org/10.1016/j.ceramint.2017.11.048
Received 29 May 2017; Received in revised form 23 October 2017; Accepted 8 November 2017
Available online 10 November 2017

while also presenting optimal clinical results [6,7].

However, Y-TZP has low fracture strength and is more prone to failures related to insufficient thickness of the fixed prostheses connector [8,9]. Also, each Y-TZP blank behaves as a single piece, and higher fracture strength does not always correspond to higher Y-TZP reliability [10,11]. Y-TZP is a very rigid, hard and brittle material whose strength is reduced by the presence of surface irregularities, internal voids and porosity [12,13]. Small surface scratches caused by finishing and polishing can initiate fractures [12]. Many characteristics may help prevent the formation and propagation of these flaws: fine-grained powders give more uniform surfaces, and reinforcement materials may act as break-off propagation. Particle or fiber reinforcement can create a toughening mechanism that is associated with cracks' bridging, but due to the chemical inertness of ceramics, the enhancement in fracture toughness obtained may be low [5]. Microcracks and defects that develop due to the thermal and mechanical processing of ceramics may significantly influence strength values [13] and especially structural reliability. The management of all manufacturing and machining steps involved is important to control the formation and distribution of defects and to lead to more predictable clinical behavior of the Y-TZP ceramic.

TiO_2 has been employed as nanoparticles or coatings in medical devices to improve mechanical properties and chemical stability [14,15]. In particular, nanotubes, like nanofibers, have a high surface area-to-volume ratio, which may lead to significant enhancements in physical and mechanical material properties [16,17]. Moreover, the hollow structure of the nanotube provides additional interlocking with the matrix through both the interior and exterior surfaces of the tubes, and the high aspect ratio provides higher interfacial interaction [17,18].

In the specialized literature, a number of studies have reported the successful association of TiO_2 nanotubes with PMMA bone cement [17] and flowable dental composites [16]. Also, the incorporation of TiO_2 nanoparticles in dental resins [19,20] and glass-ionomer cements [21] has resulted in enhanced mechanical properties. However, some studies have suggested that using nanoparticles to enhance the mechanical properties of materials may not be successful due to nanoparticle agglomeration [16,19,22], and, also, so far there are no studies reporting TiO_2 nanostructures' incorporation in ceramic materials.

Considering the high biological reactivity of TiO_2 nanotubes and the inertness of Y-TZP, and also the lack of studies on the interaction between these two materials and its consequences for ceramic material properties, the purpose of this study was to evaluate the mechanical behavior and microstructure of experimental Y-TZP ceramics with different blends (0%, 1%, 2% and 5% in volume) of TiO_2 nanotubes, controlling all manufacturing steps. The study investigated whether there would be differences in structural reliability between controlled Y-TZP blank manufacturing compared to commercial Y-TZP.

2. Material and methods

2.1. Synthesis of the TiO_2 nanotubes

The nanotubes used in this study were obtained using a method described elsewhere [15]. In summary, the specimens were prepared by mixing 12 g anatase TiO_2 (Aldrich, 99%) in 200 ml of 10 M NaOH, kept at 120 °C for 24 h in a Teflon open container, which was placed in a glycerin bath, using a mantle heater for heating. The syntheses were carried out at ambient pressure, where only precursor reagents were subjected to alkaline treatment. After the alkaline treatment, the mixture was washed with 0.1 M hydrochloric acid (HCl) and deionized water repeatedly to remove the sodium ions. Finally, the materials obtained were dried in a conventional oven at 200 °C for 24 h in open air to obtain TiO_2 nanotube powder.

Fig. 1 shows an image of the TiO_2 nanotubes obtained by TEM (CM 200, Phillips, Netherlands) with electron acceleration of 200 kV. A single sheet of spiral-wound TiO_2 results in nanotubes with, on average, 200 nm length, 20 nm thickness and 10 nm of inner diameter, each.

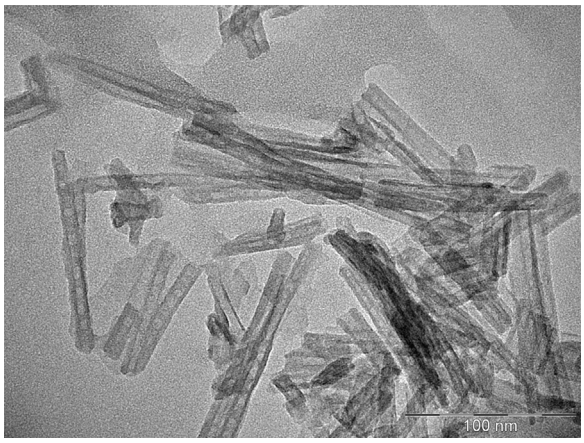

Fig. 1. TEM image of TiO_2 nanotubes obtained with average dimensions: 200 nm length, 20 nm thickness and 10 nm of inner diameter.

2.2. Specimen preparation

The Y-TZPs evaluated are described in Table 1. All zirconia-based ceramics used presented a tetragonal crystal phase stabilized with 3% mol of yttria (Y_2O_3). Only group 1 was composed of a commercially available ceramic. The other groups' ceramics were prepared from powder to sintering, controlling every step.

The experimental Y-TZP manufacturing was carried out using a process summarized in Fig. 2. The tetragonal crystal phase stabilized with 3% mol of yttria (Y_2O_3) powder (Tosoh Corporation, Tokyo, Japan; Lot. Z306234P) had grains with a surface area of 15.1 m^2/g. The solvent, binder and deflocculant agents were added to the Y-TZP powder. The powder (zirconia + nanotubes)/liquid (isopropyl alcohol) proportion was 30/70% in volume. The proportion of TiO_2 nanotubes added was calculated considering the total volume of the mixture, and the proportion of each component is presented in Table 2. Each of the components was weighed on a digital precision scale AUW220D (0.00000) (Shimadzu Corporation, Tokyo, Japan).

The jar containing zirconia balls and the mixture, except the nanotubes, was taken to a vibratory mill for 2 h for homogenization. Nanotubes were added to the appropriate groups after this mixture and were again taken to the vibratory mill with only 10% of the zirconia balls for 10 min.

Then, the mixture was poured into a glass container and dried with a heat gun at 60 °C with manual stirring until all solvent was eliminated in order to isolate the ceramic powder. The zirconia balls used in the mixture were discarded, and the powder was granulated in stainless steel sieves, meshes #50 (300 μm) and #80 (180 μm), in order to obtain dimensional homogeneity with the agglomerates and ease the weighing step.

Conformation of the ceramic discs was carried out in two steps: uniaxial and isostatic pressing. For the uniaxial pressing, the granulated powder was manually inserted in a hardened steel mold 16 mm in diameter, previously oiled with oleic oil ($C_{18}H_{34}O_2$) (Labsynth, Diadema, Brazil) and slightly vibrated for powder accommodation. To have a final thickness of 1.2 mm, considering an average sintering shrinkage of 20%, 0.75 g of ceramic powder was used for each disc. Uniaxial pressing was done in a hydraulic press at 100 MPa for 30 s maximum. In sequence, for the isostatic pressing, specimens were inserted in elastomeric balloons. The air was evacuated by a vacuum pump, and the balloons were tied tight. The balloon with the Y-TZP discs was inserted into the isostatic pressing machine and remained there for 30 s at approximately 206 MPa (30,000 psi) pressure to

Table 1
Material (Y-TZP), composition, commercial brands and experimental groups.

Groups	Material	Composition (in volume)	Commercial brand
ZC	Y-TZP IPS e.max Zircad	• 95.0% ZrO_2 (zirconium dioxide); • 5.0% of oxides [HfO_2 (hafnium dioxide) + Al_2O_3 (aluminum dioxide) + Y_2O_3 (yttrium dioxide) + other oxides].	Ivoclar Vivadent, Liechtenstein
Z0	Experimental Y-TZP no TiO_2 added	• 94.5% ZrO_2 (zirconium dioxide); • 5.3% Y_2O_3 (yttrium dioxide) + 0.2% Al_2O_3 (aluminum dioxide) + other oxides.	No commercial brand
Z1	Experimental Y-TZP 1.0% in volume TiO_2 added	• 93.6% ZrO_2 (zirconium dioxide); • 5.2% Y_2O_3 (yttrium dioxide) + 0.2% Al_2O_3 (aluminum dioxide) + other oxides; • 1.0% TiO_2.	No commercial brand
Z2	Experimental Y-TZP 2.0% in volume TiO_2 added	• 92.7% ZrO_2 (zirconium dioxide); • 5.1% Y_2O_3 (yttrium dioxide) + 0.2% Al_2O_3 (aluminum dioxide) + other oxides; • 2.0% TiO_2.	No commercial brand
Z5	Experimental Y-TZP 5.0% in volume TiO_2 added	• 89.8% ZrO_2 (zirconium dioxide); • 5.0% Y_2O_3 (yttrium dioxide) + 0.2% Al_2O_3 (aluminum dioxide) + other oxides; • 5.0% TiO_2.	No commercial brand

homogenize the compaction. After pressing, the Y-TZP green discs were 1.5 mm thick.

Green Y-TZP discs sintering was carried out in one step in atmospheric environment in a chamber furnace (Blue M Lindberg, Thermo Scientific, Waltham, USA). The sintering temperature suggested by the manufacturer of the ceramic powder is 1350 °C. In a previous study [23] that was developed in the same laboratory as the present study, sintering tests performed found that a temperature of 1350 °C led to grain size of 0.29 ± 0.08 μm and a density of 6.08 g/cm3 and for 1400 °C a grain size of 0.35 ± 0.07 μm and a density of 5.998 g/cm3. However, at 1350 °C the open pores prevailed: 0.011% at 1350° compared to 0.0028% at 1400°. Considering that dental applications occur under extreme humidity, a compromise temperature between smaller grain sizes with higher density and lower open porosity had to be used. So, the sintering temperature applied for these ceramic specimens was 1380 °C. The sintering regimen carried out for the experimental ceramic is explained in Fig. 3.

For ZC, specimens were first machined from pre-sintered blanks that were prepared in order to reach the same dimensions of specimens produced with experimental Y-TZP (12 mm diameter × 1.2 mm thickness). Then, they were sintered according to the following regimen: heating rate of 12 °C/min from room temperature to 1500 °C, 120 min at 1500 °C, cooling rate of 12 °C/min and 1 h and 27 min of waiting time, with a total cycle of 7 h and 52 min.

2.3. Biaxial flexural strength

The test was conducted according to the standard ISO 6872:2015 [24] (n = 30) and Weibull analysis was one of the main goals of this evaluation. For the support of the test specimen, an apparatus consisting of three hardened steel balls with a diameter of 3.5 mm, positioned 120° apart on a support circle with a diameter of 10 mm, was used. The disc specimens (12 × 1.2 mm) were cleaned with isopropyl alcohol and placed concentrically on these supports, and the load was applied with a flat punch with a diameter of 1.4 mm at the center of the specimen at a 0.5 mm/min speed in a universal testing machine (Kratos X2000MP, Shimadzu, Kyoto, Japan). From the equation below, the biaxial flexural strength (σ) was calculated in megapascals (MPa): $\sigma = -0{,}2387\ P(X-Y)/b^2$, where σ is the maximum center tensile stress, in megapascals; P is the total load causing fracture, in Newtons; and X and Y were calculated from the equations $X = (1 + v)\ln(r_2/r_3)^2 + [(1 - v)/2](r_2/r_3)^2$ and $Y = (1 + v)\ln(r_1/r_3)^2 + [(1 - v)/2](r_1/r_3)^2$, in which v is Poisson's ratio = 0,25; r_1 is the radius of support circle, in millimeters; r_2 is the radius of loaded area, in millimeters; r_3 is the radius of specimen, in millimeters and b is the specimen thickness at fracture origin, in millimeters.

2.4. Fractographic analysis

For the fractographic analysis, fractured surfaces of the specimens were cleaned first in water for 15 min, in an ultrasonic bath, followed by 15 min of immersion in 92.8% ethanol. The surfaces of the specimens were first examined under a stereomicroscope (Dino-Lite AM313T, An Mo Electronics Corporation, New Taipei City, Taiwan) to determine the location of the fracture origin. Five specimens from each group (n = 5) were randomly selected and gold-coated for analysis in a SEM (JSM 5600LV, JEOL, Tokyo, Japan). Qualitative analyses of the fracture surfaces were completed at 35× and 500× magnification. EDX (X Oxford Instruments X-Max^N, Abingdon, United Kingdom) was used to further analyze the fracture surfaces for Ti and Zr contents.

2.5. Microstructure

Y-TZP surface microstructure was evaluated in FE-SEM (JSM-IT300,

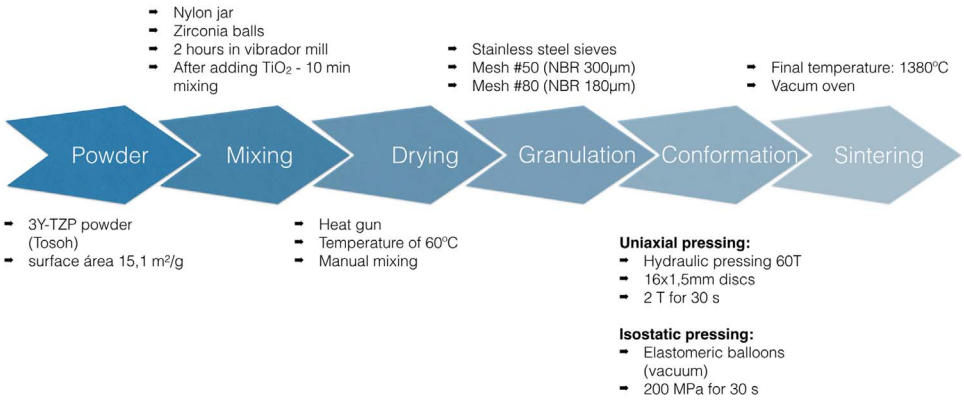

Fig. 2. Y-TZP manufacturing from the zirconium oxide powder.

Table 2
Zirconia powder, nanotubes, solvents, binders, and deflocculants used in the mixture.

Component	Function	Commercial brand	Density (g/cm^3)	Proportion (%)
Zirconia powder	Ceramic powder	Tosoh Corporation (Tokyo, Japan)	6.05	30% (total volume)
PABA (4-Aminobenzoic acid)	Deflocculant	Vetec Química Fina (Rio de Janeiro, Brazil)	1.37	0.5% (ZrO_2 weight)
Isopropyl alcohol	Solvent	Labsynth (Diadema, Brazil)	0.78	70% (total volume)
PVB (Polyvinyl butyral)	Binder	Butvar B-98, Sigma Aldrich (Saint Louis, USA)	1.1	2% (ZrO_2 weight)
TiO_2 nanotubes	Additive	No commercial brand	4.23	1, 2 or 5% (total volume)

JEOL, Tokyo, Japan) to analyze the grain size. First, the specimens were polished with sandpaper on grits #150, #240, #320, #400, #600, #800 and #1200. They were polished for 5 min with each different grit. Then, they were polished with felt discs and diamond abrasive paste of 4 μm, 2 μm and 1 μm in a semiautomatic sander (EXACT, Nordestedt, Schleswing-Holstein, Germany). After polishing, they were submitted to thermal treatment in a sintering oven (Blue M Lindberg, Thermo Scientific, Waltham, USA) according to the following regimen: from room temperature to 600 °C at a rate of 4 °C/min, from 600 °C to 1000 °C at 5 °C/min, from 1000 °C to 1300 °C at 10 °C /min and 6 min at 1300 °C. After this process, the grain boundaries were exposed and then gold-coated. Grain sizes were measured using the Image J program (version 1.47, Wayne Rasband, National Institute of Health, USA).

2.6. X-ray diffraction

XRD was carried out on a Siemens D-5000 instrument (Bruker, Billerica, USA), in the Bragg θ–2θ geometry, equipped with a graphite monochromator and Cu Kα radiation (λ = 1,5418 Å), operating with a voltage of 40 kV and an emission current of 40 mA. Data were obtained in step times of 1.0 s and step sizes of 0.030° (2θ) from 20 to 80°.

2.7. Statistical analysis

Statistical analysis was performed with the software SPSS 19.0 for Windows (SPSS Inc., IBM, Chicago, USA). Biaxial flexural strength and grain size values were subjected to the Kolmogorov-Smirnov and Shapiro-Wilk normality tests. Levene's test was performed to verify the homogeneity of variances. Data for flexural strength passed all these tests, so they were analyzed by ANOVA at the $\alpha = 0.05$ significance level, followed by Tukey's test for comparisons between groups. Data of grain sizes did not pass normality and homogeneity tests and were then analyzed by Kruskal-Wallis at the $\alpha = 0.05$ significance level and by Dunn's test for multiple comparisons.

Biaxial flexural strength values were recorded and used to determine the Weibull distribution fit for the groups (Weibull 7++, Reliasoft, Tucson, USA) by the maximum likelihood method. Weibull modulus (m) and characteristic strength (σ_0) were determined for each group, and a contour plot was used to examine differences between groups ($p < 0.05$). A reliability plot was also used for group comparisons.

3. Results and discussions

3.1. Biaxial flexural strength

Values of mean and standard deviation for biaxial flexural strength (σ), as well as the minimum and maximum values, are described in Table 3. Group ZC presented the highest flexural strength among all groups, with a significant difference from the others ($p < 0.05$), followed by groups Z0, Z2, Z1 and Z5, respectively.

Fig. 4 shows the Weibull probability plot, with fracture stress as a function of the probability of fracture for the different Y-TZPs. It can be noted that all groups presented linear distribution of fracture stress values, although a few values deviated from the probability line. Values found for σ_0 and m are shown in the Weibull two-parameter contour plot (Fig. 5). It was possible to note that ZC showed significantly higher σ_0 compared to other groups; however, its m was lower. Additionally, Z0 presented a non-overlapping confidence bound, with σ_0 lower than ZC but higher than the other groups; its m was higher than that of ZC.

In this study, the m value for ZC (7.9) was lower and the σ_0 value (948.9) was higher than in the other groups. This shows that the variation of strength values was high, which could mean that flaw sizes are quite variable and fractures could occur in a large portion of the specimens [25]. Group Z0 presented the highest m value (11.2) and, hence, less variation in strength, which could mean that this material presented a smaller error range, flaws similar in size and distribution and, therefore, greater structural reliability [25,26], leading to the assumption that the manufacturing steps were well controlled. Also, soft machining carried out in the ZC group may introduce residual surface compressive stresses that lead to increased strength, but it could also create deep defects in the ceramic structure, which would act as stress-concentrating areas or flaws, leading to lower reliability [13].

Groups Z1 ($m = 8.7$) and Z5 ($m = 9.3$) presented overlapping confidence bounds in the contour plot and higher m values than ZC and Z2, even though they presented lower σ_0 and a microstructure with a greater amount of flaws. It could be understood that even though they presented potentially critical flaws (pores), the ceramic microstructure homogeneity was controlled and ensured uniform stress distribution [27]. As in most groups, the m values were similar (except for Z0). A flaw difference may not be the only explanation for strength differences; they are probably also due to differences in toughness, which are related to the manufacturing process, as well as parameters of stress corrosion and strength level [25,27].

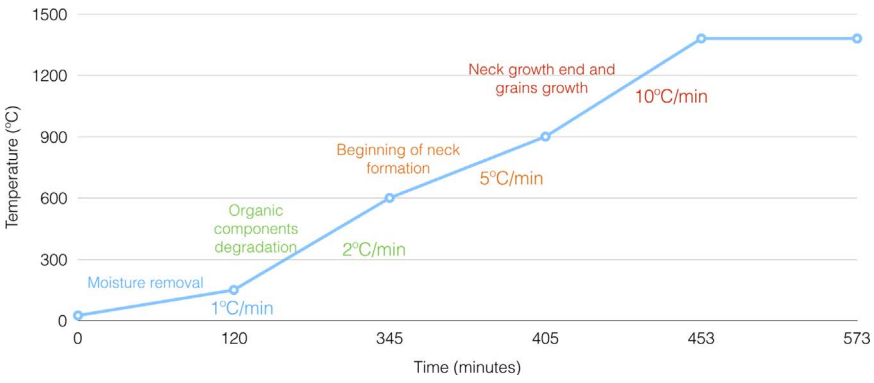

Fig. 3. Sintering regimen executed with description of Y-TZP characteristics in each of these phases.

Table 3
Values of flexural strength σ ± SD and the σ minimum and σ maximum found for each group (n = 30).

Groups	ZC	Z0	Z1	Z2	Z5
σ (MPa)	896.73 ± 122.70^{A}	577.67 ± 62.26^{B}	477.32 ± 75.65^{C,D}	492.25 ± 63.19^{C}	437.18 ± 53.55^{D}
σ_{min} (MPa)	593.82	442.07	228.91	389.98	339.77
σ_{max} (MPa)	1195.98	673.72	576.74	644.94	543.50

Values followed by different superscript letters show significant difference among groups ($p < 0.05$).

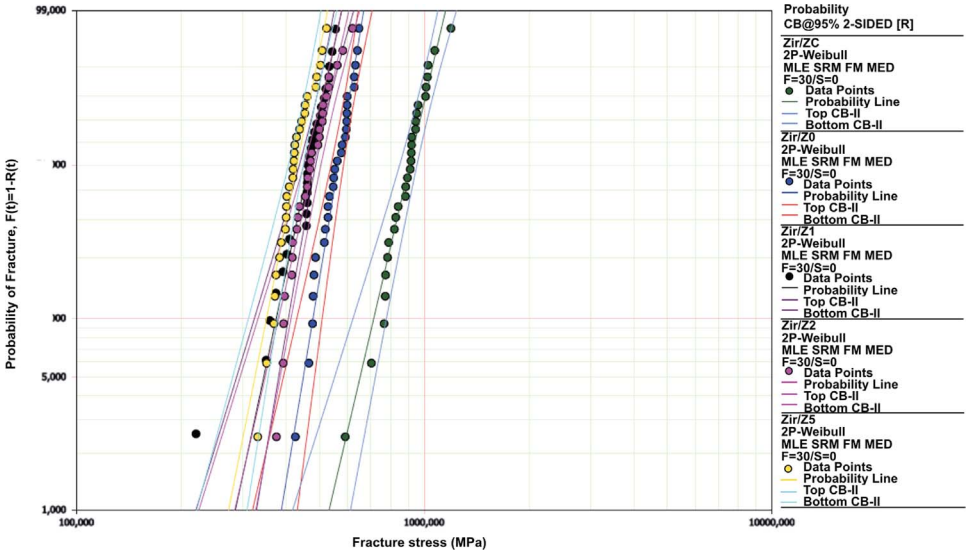

Fig. 4. Weibull plot presenting fracture stress as a function of probability of fracture.

3.2. Fractographic analysis

Images obtained through SEM analysis of the fractured specimens are shown in Fig. 6(A–J). Figures at 35× show the entire fractured area of the disc, with indication of the telltale marks found on these specimens: compression curls (cc) opposite to the origin of failure, mirror regions (m), hackle lines (hl) and wake hackle lines (wh) indicating the direction of crack propagation (arrows) and pores (p) as the main flaw types observed in all groups. The first step in fractography is to find these telltale marks that will help understand the reason for the failure. The polycrystalline nature of ceramics masks most of these details, especially fracture mirrors, relatively smooth areas that should be identified if it is necessary to find the fracture origin [28]. Accordingly, in ZC and Z0 it was easier to identify the mirrors (Figs. 6A, B, C, D), while in Z5 (Figs. 6I and J) it was very hard to do so. According to Quinn [28], mirrors may not be detectable in coarser grained materials or those with more than 10% porosity, justifying this difficulty.

Microcracks and defects that intrinsically grow during manufacturing processes can reduce the total area in which stresses are generated, acting as stress concentrators [5,12,13,25,27]. It can be noted in Fig. 6 that as the concentration of nanotubes increased, the amount of visible pores in the fracture area also increased. EDX analysis showed that these pores were not empty; they had a high Ti concentration inside, not in the nanotube form (Fig. 7), probably melted due to the high temperatures of Y-TZP sintering (1350 °C). Although agglomeration of nanomaterials is often reported in the literature [17,22], the nanotube form probably favored the better distribution of these structures in the ceramic, which is proved by the high *m* values

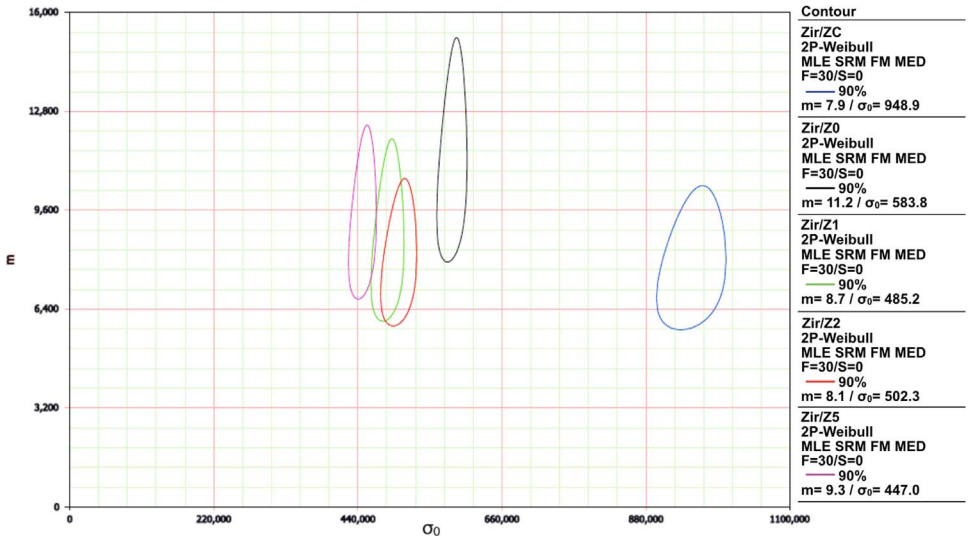

Fig. 5. Contour plot with 90%confidence intervals for the σ_0 and *m* parameters.

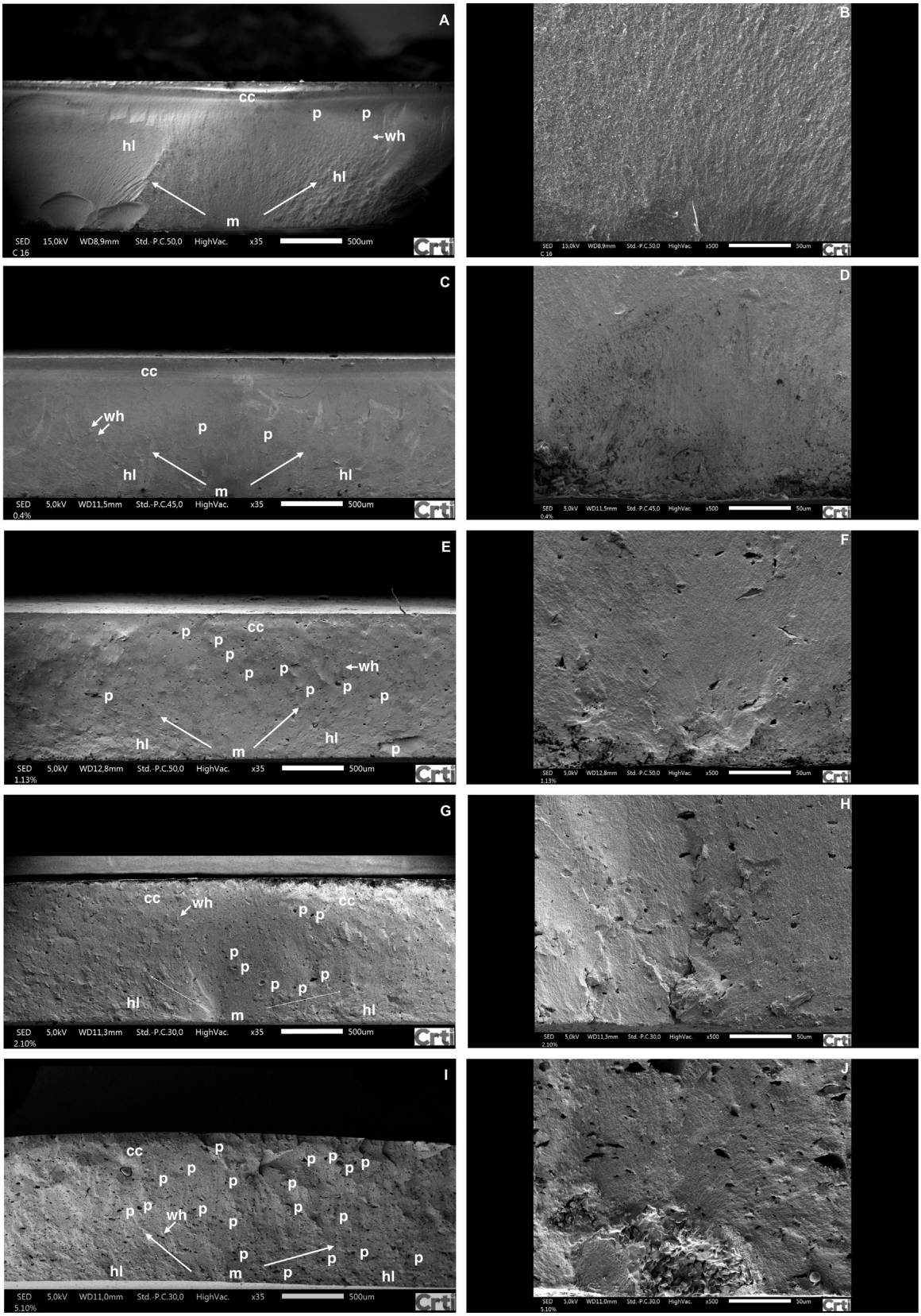

Fig. 6. Fractography images of specimens tested. On the fractured surfaces of a specimen on group ZC (6A – 35× and 6B – 500×) and of group Z0 (6C – 35× and 6D – 500×) is easy to identify the telltale marks: compression curls (cc) opposite to the origin of failure, mirror regions (m) surrounding the origin, hackle lines (hl) and wake hackle lines (wh) indicating the direction of crack propagation (arrows) and pores (p). On the fractured surfaces of specimens on groups Z1 (6E – 35 × and 6F – 500×) and Z2 (6G – 35× and 6H – 500×) it is harder to see the telltale marks and more pores (p) are visible in the surface, the mean pore sizes are 4.15 μm and 5.63 μm, for Z1 and Z2, respectively. Fractured surface of a group Z5 specimen (6I – 35× and 6J – 500×) is much harder to identify this marks and more pores in a bigger size (mean size 10.76 μm) are observed.

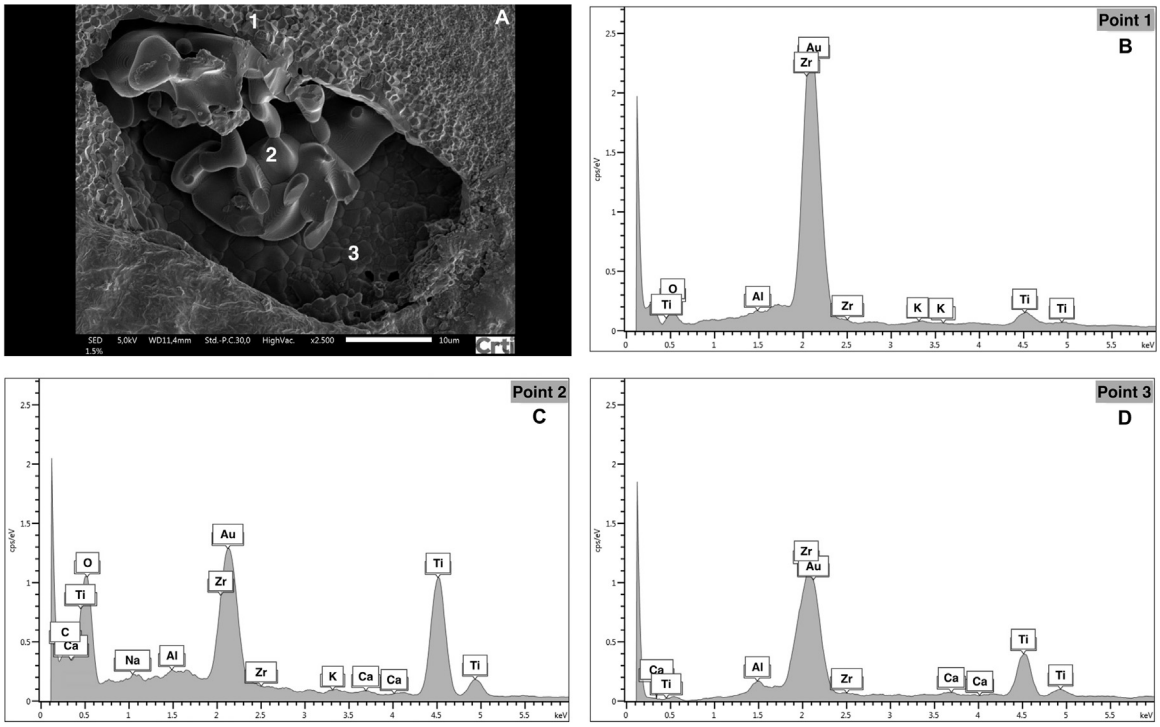

Fig. 7. Close up image (2500×) of a pore in a specimen from group Z1 with indication of areas of EDX analysis (7A). EDX graphic from point number 1 showing the great presence of zirconium, almost no titanium (7B). EDX graphic from point number 2 showing the presence of zirconium and also titanium (7C). EDX graphic from point number 3 showing the presence of zirconium and less titanium (7D).

obtained. Furthermore, due to Y-TZP inertness [29], there is no chemical reaction between nanotubes and the ceramic, creating a very poor interaction, so the reinforcement nanomaterial may act like pores when stress is applied, leading to lower flexural strength [17,22].

Figures at 500× show a close-up image of the mirror regions and the possible critical defects of each fractured specimen. When stress is applied, a material is more prone to break from a sharp flaw than from a blunt flaw, such as a pore, of a similar size [25]. In this study, most flaws observed in the experimental ceramics were pores, probably introduced during processing as no mechanical means such as grinding or polishing were used in ceramic production. The mean pore size was measured with Image J (version 1.47, Wayne Rasband, National Institute of Health, USA) in the 500× images, and the means obtained were Z1: 4.15 μm; Z2: 5.63 μm and Z5: 10.76 μm. These pores were more evident as the nanotube concentration was augmented and not bigger than 20 μm, probably associated with the nanotubes' melting as well [25].

3.3. Microstructure

The mean grain sizes and standard deviation for each group are presented in Table 4. The FE-SEM images obtained for each group are presented in Fig. 8(A–E). It is well established that grain size strongly influences the transformability, toughness and aging resistance of Y-TZP [5,29–31]. In the FE-SEM images obtained, groups ZC and Z0 presented the lowest mean grain sizes, with no significant difference between them ($p > 0.05$). This finding shows that the ceramics produced by the authors presented good crystal size when compared to the commercial ceramic.

With the addition of TiO_2 nanotubes, the grain size slightly increased, with a significant difference from Z0 in all concentrations ($p < 0.05$). (Table 4). Camposilvan et al. [32] presented similar results when cerium oxide (CeO_2) was added to Y-TZP, and they related the grain growth to both (1) the reduction of yttria in tetragonal grains, as yttria segregates at grain boundaries, exerting a drag force against their mobility; and (2) the generation of more yttria-rich cubic grains, which grow faster. Over a critical grain size (> 1000 nm), the Y-TZP is less stable and more susceptible to spontaneous t-m transformation during cooling, while smaller grain sizes (< 200 nm) are associated with lower transformation rates, even under stress [13,30,31,33]. According to ISO standard 13356:2008 [34], the mean grain size (expressed as the mean linear-intercept distance) should not exceed 400 nm, even for the biggest mean grain sizes; all groups in this study followed this recommendation.

Table 4
Mean grain sizes (± SD) for the different Y-TZP in nm.

Groups	ZC	Z0	Z1	Z2	Z5
Mean	284.57[a,b]	279.05[a]	302.81[b,c]	307.61[b,c]	325.68[c]
SD	108.50	116.90	117.27	131.14	143.14

Values followed by different superscript letters show significant difference among groups ($p < 0.05$).

3.4. X-ray diffraction

XRD results are presented in Fig. 9A and B. Peaks observed for commercial Y-TZP and experimental Y-TZP are very similar. The addition of TiO_2 nanotubes did not cause any detectable structural modification or phase segregation in the Y-TZP. It can also be observed that with the addition of nanotubes, there was a little increase in the monoclinic phase of Y-TZP, as the peak observed in that region was very low in Z0 and slightly increased according to the increase in concentration of TiO_2 nanotubes. This is a positive result as predominance of the tetragonal phase in the Y-TZP crystal structure is essential for transformation toughening to occur [13].

This zirconia produced with the different blends of TiO_2, with different pore and grain sizes, might be further studied as a pre-

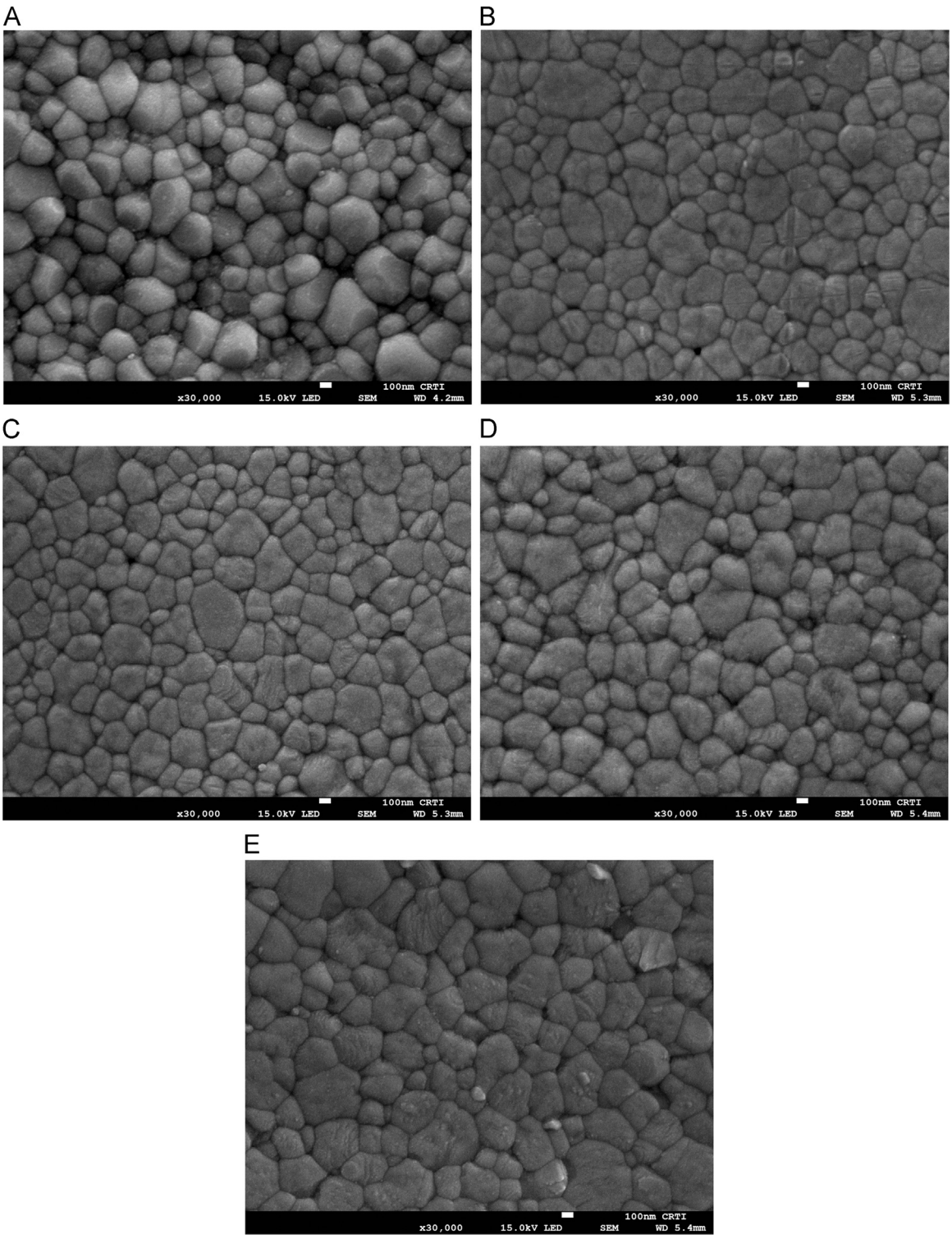

Fig. 8. FE-SEM image of each group showing the grain sizes and distributions, ×30,000. ZC's image (8A) presents grains very different from the other groups although in similar sizes to Z0 (8B) grains. With nanotubes concentration increase, the grain sizes also increased and it can be seen in Fig. 8C, D and E, representing groups Z1, Z2 and Z5, respectively.

programmed material for specific indications due to the nanometric size of the pores obtained and the high *m* values, indicating high structural reliability, especially of blends of TiO_2 at 1% and 5%.

4. Conclusion

Y-TZP blanks produced while controlling all manufacturing steps presented good microstructure when compared to commercial Y-TZP, with grain sizes very similar to each other. Experimental ceramics also presented higher *m* values and, hence, greater structural reliability than the commercial ceramic. TiO_2 nanotube additions in different blends (1%, 2% and 5% in volume) influenced Y-TZP properties, leading to lower flexural strength but *m* values higher than in commercial Y-TZP. A large number of pores containing Ti were observed as the nanotube concentration was higher, and it probably positively influenced its structural reliability (*m*).

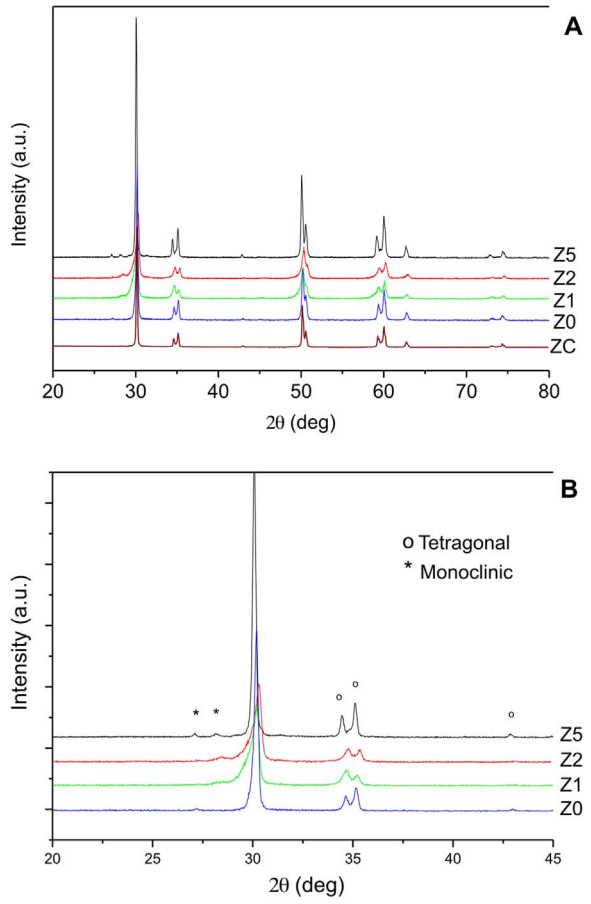

Fig. 9. Graphics presenting the X-ray diffraction results observed for each group of Y-TZP. No structural changes or segregations after nanotubes addition can be noted (9A). In the 20° to 45° interval the nanotubes incorporation made the monoclinic phase noticeable in a small amount (9B).

Acknowledgements

The authors would like to thank the financial support of the FAPESP - São Paulo Research Foundation process numbers: 2011/18061-0 and 2013/07296-2 (CDMF/CEPID/FAPESP).

References

[1] W.D. Callister Jr., D.G. Rethwisch, Materials Science and Engineering, An Introduction, ninth ed., John Wiley & Sons, Hoboken, 2007.
[2] C. Gautam, J. Joyner, A. Gautam, J. Rao, R. Vajtai, Zirconia based dental ceramics: structure, mechanical properties, biocompatibility and applications, Dalton Trans. 45 (2016) 19194–19215.
[3] C. Piconi, G. Maccauro, Zirconia as a ceramic biomaterial, Biomaterials 20 (1999) 1–25.
[4] T. Derand, M. Molin, K. Kvam, Bond strength of composite luting cement to zirconia ceramic surfaces, Dent. Mater. 21 (2005) 1158–1162.
[5] B. Basu, Toughening of yttria-stabilised tetragonal zirconia ceramics, Int. Mater. Rev. 50 (2005) 239–256.
[6] I. Sailer, A. Fehér, F. Filser, L.J. Gauckler, H. Lüthy, C.H. Hämmerle, Five-year clinical results of zirconia frameworks for posterior fixed partial dentures, Int. J. Prosthodont. 20 (2007) 383–388.
[7] R. Sorrentino, G. De Simone, S. Tetè, S. Russo, F. Zarone, Five-year prospective clinical study of posterior three-unit zirconia-based fixed dental prostheses, Clin. Oral. Investig. 16 (2012) 977–985.
[8] F. Beuer, D. Edelhoff, W. Gernet, J.A. Sorensen, Three-year clinical prospective evaluation of zirconia-based posterior fixed dental prostheses (FDPs), Clin. Oral. Investig. 13 (2009) 445–451.
[9] C. Larsson, L. Holm, N. Lövgren, Y. Kokubo, P. Vult Von Steyern, Fracture strength of four-unit Y-TZP FPD cores designed with varying connector diameter. An in-vitro study, J. Oral. Rehabil. 34 (2007) 702–709.
[10] W.S. Lin, C. Ercoli, C. Feng, D. Morton, The effect of core material, veneering porcelain, and fabrication technique on the biaxial flexural strength and weibull analysis of selected dental ceramics, J. Prosthodont. 21 (2012) 353–362.
[11] R.G. Fonseca, F.O. Abi-Rached, F.S. da Silva, B.A. Henriques, L.A. Pinelli, Effect of surface and heat treatments on the biaxial flexural strength and phase transformation of a Y-TZP ceramic, J. Adhes. Dent. 16 (2014) 451–458.
[12] J.F. McCabe, A.W.G. Walls, Applied Dental Materials, ninth ed., Blackwell Publishing Ltda, Hong Kong, 2008.
[13] C.A.M. Volpato, L.G.D. Garbelotto, M.C. Fredel, F. Bondioli, Application of zirconia in dentistry: biological, mechanical and optical considerations, in: C. Sikalidis (Ed.), Advances in Ceramics - Electric and Magnetic Ceramics, Bioceramics, Ceramics and Environment, InTech, 2011, , http://dx.doi.org/10.5772/21630.
[14] J. Ai, E. Biazar, M. Jafarpour, M. Montazeri, A. Majdi, S. Aminifard, M. Zafari, H.R. Akbari, H.G. Rad, Nanotoxicology and nanoparticle safety in biomedical designs, Int. J. Nanomed. 6 (2011) 1117–1127.
[15] L.B. Arruda, C.M. Santos, M.O. Orlandi, W.H. Schreiner, P.N. Lisboa-Filho, Formation and evolution of TiO2 nanotubes in alkaline synthesis, Ceram. Int. 41 (2015) 2884–2891.
[16] M.O. Dafar, M.W. Grol, P.B. Canham, S.J. Dixon, A.S. Rizkalla, Reinforcement of flowable dental composites with titanium dioxide nanotubes, Dent. Mater. 32 (2016) 817–826.
[17] S.M. Khaled, R.J. Miron, D.W. Hamilton, P.A. Charpentier, A.S. Rizkalla, Reinforcement of resin based cement with titania nanotubes, Dent. Mater. 26 (2010) 169–178.
[18] C.X. Cui, X. Gao, Y.M. Qi, S.J. Liu, J.B. Sun, Microstructure and antibacterial property of in situ TiO(2) nanotube layers/titanium biocomposites, J. Mech. Behav. Biomed. Mater. 8 (2012) 178–183.
[19] J. Sun, A.M. Forster, P.M. Johnson, N. Eidelman, G. Quinn, G. Schumacher, X. Zhang, W.L. Wu, Improving performance of dental resins by adding titanium dioxide nanoparticles, Dent. Mater. 27 (2011) 972–982.
[20] C.M. Ramos-Tonello, P.N. Lisboa-Filho, L.B. Arruda, C.K. Tokuhara, R.C. Oliveira, A.Y. Furuse, J.H. Rubo, A.F.S. Borges, Titanium dioxide nanotubes addition to self-adhesive resin cement: effect on physical and biological properties, Dent. Mater. S0109–5641 (2017) (30093-3).
[21] E. Gjorgievska, G. Van Tendeloo, J.W. Nicholson, N.J. Coleman, I.J. Slipper, S. Booth, The incorporation of nanoparticles into conventional glass-ionomer dental restorative cements, Microsc. Microanal. 21 (2015) 392–406.
[22] J. Hill, J. Orr, N. Dunne, In vitro study investigating the mechanical properties of acrylic bone cement containing calcium carbonate nanoparticles, J. Mater. Sci. Mater. Med. 19 (2008) 3327–3333.
[23] A.A. Fiocchi, Science and Technology of Ultra-precision Manufacturing of Advanced Ceramics: Ud-lap Grinding of Flat Surfaces of Tetragonal Zirconia Policristal Estabilized with Itria. 327 (Theses), Engineering School of São Carlos. University of São Paulo, 2014, http://dx.doi.org/10.11606/T.18.2014.tde-30032015-094410 (Acessed 19 October 2017), http://www.teses.usp.br/teses/disponiveis/18/18146/tde-30032015-094410/publico/Tese_Arthur_Alves_Fiocchi_corrigida.pdf.
[24] International Standard ISO 6872, Dentistry – Ceramic Materials, International Standards Organization, Geneva, Switzerland, 2015.
[25] J.B. Quinn, G.D. Quinn, A practical and systematic review of Weibull statistics for reporting strengths of dental materials, Dent. Mater. 26 (2010) 135–147.
[26] S.E. Elsaka, A.M. Elnaghy, Mechanical properties of zirconia reinforced lithium silicate glass-ceramic, Dent. Mater. 32 (2016) 908–914.
[27] A.D. Bona, K.J. Anusavice, P.H. Dehoff, Weibull analysis and flexural strength of hot-pressed core and veneered ceramic structures, Dent. Mater. 19 (2003) 662–669.
[28] G.D. Quinn, Fractography of Ceramics and Glasses, second ed., National Institute of Standards and Techonology, Washington, 2016.
[29] J. Cotič, P. Jevnikar, A. Kocjan, T. Kosmač, Complexity of the relationships between the sintering-temperature-dependent grain size, airborne-particle abrasion, ageing and strength of 3Y-TZP ceramics, Dent. Mater. 32 (2016) 510–518.
[30] P. Palmero, Structural ceramic nanocomposites: a review of properties and powders' synthesis, Methods Nanomater. 5 (2015) 656–696.
[31] C.M. Ramos, P.F. Cesar, E.A. Bonfante, J.H. Rubo, L. Wang, A.F. Borges, Fractographic principles applied to Y-TZP mechanical behavior analysis, J. Mech. Behav. Biomed. Mater. 57 (2016) 215–223.
[32] E. Camposilvan, F.G. Marro, A. Mestra, M. Anglada, Enhanced reliability of yttria-stabilized zirconia for dental applications, Acta Biomater. 17 (2015) 36–46.
[33] J. Li, Z. Tang, Z. Zhang, S. Luo, Study of factors influencing the microstructure and phase content of ultrafine Y-TZP, Mater. Sci. Eng. B. 99 (2003) 321–324.
[34] International Standard ISO 13356, Implants for Surgery – Ceramic Materials Based on Yttria-stabilized Tetragonal Zirconia (Y-TZP), International Standards Organization, Switzerland, Geneva, 2015.